

AD-A034 543

HONEYWELL INC MINNEAPOLIS MINN SYSTEMS AND RESEARCH --ETC F/6 1/3
DEVELOPMENT OF A HYDROFLUIDIC VERNIER ROCKET CONTROL SYSTEM FOR--ETC(U)

DEC 76 R V BURTON , R B BEALE

N00019-76-C-0374

NL

UNCLASSIFIED

F0440-FR

1 OF
AD
A034543



END

DATE

FILMED

2-77

ADA 034543

UNCLASSIFIED

SECURITY CLASSIFICATION OF THIS PAGE (WHEN DATA ENTERED)

REPORT DOCUMENTATION PAGE		READ INSTRUCTIONS BEFORE COMPLETING FORM		
14 ④	REPORT NUMBER F0440-FR 77-SRC/1	2. GOVT ACCESSION NUMBER	3. RECIPIENT'S CATALOG NUMBER ⑨	
6 ⑥	4. TITLE (AND SUBTITLE) DEVELOPMENT OF A HYDROFLUIDIC VERNIER ROCKET CONTROL SYSTEM FOR EJECTION SEAT STABILIZATION.	5. TYPE OF REPORT & PERIOD COVERED Final Report. 1 March 1976 - 1 November 1976	6. PERFORMING ORG. REPORT NUMBER 77SRC1	
10 ⑩	7. AUTHOR(S) R. V. Burton, R. B. Beale	8. CONTRACT OR GRANT NUMBER(S) N00019-C-0374	76 NEW	
	9. PERFORMING ORGANIZATION'S NAME/ADDRESS Honeywell Inc., Systems & Research Center 2600 Ridgway Parkway Minneapolis, Minnesota 55413	10. PROGRAM ELEMENT, PROJECT, TASK AREA & WORK UNIT NUMBERS 62715N F53-532-403		
	11. CONTROLLING OFFICE NAME/ADDRESS Naval Air Systems Command/Engineering Div AIR-52022E (W. Loughrey) Washington, D. C.	12. REPORT DATE Dec 1976		
	14. MONITORING AGENCY NAME/ADDRESS (IF DIFFERENT FROM CONT. OFF.) ⑫ 57p.	13. NUMBER OF PAGES 63		
		15. SECURITY CLASSIFICATION (OF THIS REPORT) Unclassified	15a. DECLASSIFICATION/DOWNGRADING SCHEDULE N/A	
	16. DISTRIBUTION STATEMENT (OF THIS REPORT) Approved for public release; distribution unlimited.	15. N00019-76-C-0374		
	17. DISTRIBUTION STATEMENT (OF THE ABSTRACT ENTERED IN BLOCK 20, IF DIFFERENT FROM REPORT) ⑯ F53532	⑰ WF53532403		
	18. SUPPLEMENTARY NOTES			
	19. KEY WORDS (CONTINUE ON REVERSE SIDE IF NECESSARY AND IDENTIFY BY BLOCK NUMBER) Ejection Seat Fluidic Hydrofluidic Thrust Vector Control	Vortex Rate Sensor Vernier Rocket Servoactuator Servovalve	Control Valve Compensation Lag-Lead Integrator	Stabilization Attitude Control
10/1983 REV 11/74	20. ABSTRACT (CONTINUE ON REVERSE SIDE IF NECESSARY AND IDENTIFY BY BLOCK NUMBER) A feasibility demonstration model of a fluidic thrust vector control (FTVC) system was designed, fabricated, and tested for pitch stabilization of ejection seats using the STAPAC vernier rocket. The control system includes a rate sensor, amplifier, attitude memory, and a position-controlled hydrofluidic servoactuator. The measured dynamic response of the control system closely matched the theoretical specifications for stable attitude control of the seat. The hardware was tested on a hydraulic rate table without rocket firing.			

402 349
LB

TABLE OF CONTENTS

	Page
SECTION I.	INTRODUCTION AND SUMMARY
	6
	Control System Concept
	6
	Performance Results
	8
SECTION II.	CONTROL SYSTEM DEVELOPMENT
	16
	Controller Logic Concept
	16
	Breadboard FTVC Preliminary Test
	19
	FTVC Final Test Results
	22
SECTION III.	HYDROFLUIDIC SERVOACTUATOR DEVELOPMENT
	31
	Servoactuator Concept
	31
	Principles of Operation
	33
	Performance Requirements
	35
	Preliminary Test Results
	37
	Servoactuator Design
	38
	Final Test Results
	46
SECTION IV.	CONCLUSIONS
	54
REFERENCES	57
DISTRIBUTION LIST	58

ACCESSION for	
NTIS	White Section
DOC	Buff Section
UNANNOUNCED	
JUSTIFICATION.....	
BY.....	
DISTRIBUTION/AVAILABILITY CODES	
Dist.	Avail. and / or Special
A	

LIST OF ILLUSTRATIONS

Figure		Page
1	Breadboard Feasibility Demonstrator	7
2	Component Block Diagram	9
3a	Detailed Schematic of NAVAIR Breadboard Fluidic Thrust Vector Control	10
3b	Controller Schematic Showing Internal Resistance Network	11
4	Comparison of Measured and Ideal Controllers	14
5	Dynamic Response Design Goal for NAVAIR Fluidic Thrust Vector Control System	18
6	Experimental Dynamic Response for NAVAIR Fluidic Thrust Vector Control	21
7	NAVAIR Breadboard FTVC--Steady State Gain	24
8	NAVAIR Breadboard FTVC Dynamic Response (Design Goal vs. Measured)	28
9	NAVAIR Breadboard FTVC Transient Response for 20 Degree Seat Angle Change	29
10	Servoactuator System Diagram	32
11	Hydrofluidic Servoactuator Schematic	34
12	Scale Factor--ACH104A1002 Hydrofluidic Servoactuator, 500 psig Supply Pressure	39
13	Scale Factor--ACH104A1002 Hydrofluidic Servoactuator, 1000 psig Supply Pressure	40
14	Scale Factor--ACH104A1002 Hydrofluidic Servoactuator, 1500 psig Supply Pressure	41

LIST OF ILLUSTRATIONS (Concluded)

Figure		Page
15	Scale Factor--ACH104A1002 Hydrofluidic Servoactuator, 2000 psig Supply Pressure	42
16	Dynamic Response--Pilot Production ACH104A1002 Hydrofluidic Servoactuator	43
17	Servo Scale Factor with Hydraulic Bench Input	50
18	Measured Dynamic Response--NAVAIR ACH104A Hydrofluidic Servoactuator	51
19	Servo Scale Factor with Controller Input	52

LIST OF TABLES

Table		Page
1	Control System Performance	12
2	Modified ACH104A (NAVAIR) Hydrofluidic Servoactuator Test Results	48

SECTION I

INTRODUCTION AND SUMMARY

CONTROL SYSTEM CONCEPT

A fluidic thrust vector control (FTVC) system was designed, fabricated, and tested to stabilize ejection seats in accordance with the performance criteria defined in a previous contract (Reference 1). The control system includes a rate sensor, amplifier, lag-lead compensation, position-controlled servo-actuator, and a vernier rocket. The measured dynamic response of the control system closely matched the theoretical specifications for stable attitude control of the seat. This attitude control is significantly different from the pitch damping control which is obtained with the same vernier rocket in the STAPAC mechanical control system. The breadboard system met or exceeded the performance requirements of time constants, gain, bandwidth, torque, slew rate, deflection angle, and attitude reference bias. The hardware was tested on a hydraulic rate table without rocket firing. This hardware is now ready for hot gas bench tests and seat launching tests.

A picture of the hardware is shown in Figure 1. This hardware is a breadboard feasibility demonstrator and is considerably larger than a properly packaged unit would be. The bulk of the unit is manifolding which is flexible enough to take different numbers of amplifiers. The memory capacitor piston is large enough to obtain memory time constants up to 40 sec. However, this hardware is an effective design tool and it fits on the ESCAPAC seat in place of the STAPAC system.

Figure 1. Breadboard Feasibility Demonstrator



The system is very rugged. It can withstand a long shelf life because it consists primarily of empty fluid lines running through steel and aluminum. There is a minimum of moving parts. The actuator shaft and the piston capacitor are the only sliding or rotating contacts. In the future the piston capacitor will be replaced with a diaphragm or bellows to increase the shelf life reliability.

A block diagram showing how the control system interfaces with the seat in an outer control loop is described in Figure 2. The θ_{BIAS} term is an attitude reference which can be set to obtain a desired pitch attitude. This setting is made with a fixed orifice in the breadboard hardware; an electromagnetic valve could be used for variable settings.

The schematic of the fluidic circuit is shown in Figures 3a and 3b. Note that the rate signal bypasses the capacitor to achieve attitude control in combination with rate damping. Note also the three-stage fluidic servovalve with position feedback. The pressure signal for position feedback is obtained from a slot in the actuator shaft.

PERFORMANCE RESULTS

The dynamic performance requirements were defined in a previous study (Reference 1) using simulations of seat trajectories and a linearized stability analysis of seat response. Table 1 lists the major parameters and compares the design goals and measured values. Note that the actuator is considerably larger and more powerful than required. The controller gains and time constants are very close to the design goals. The actuator and rate sensor response are slightly lower than the design goals, causing the

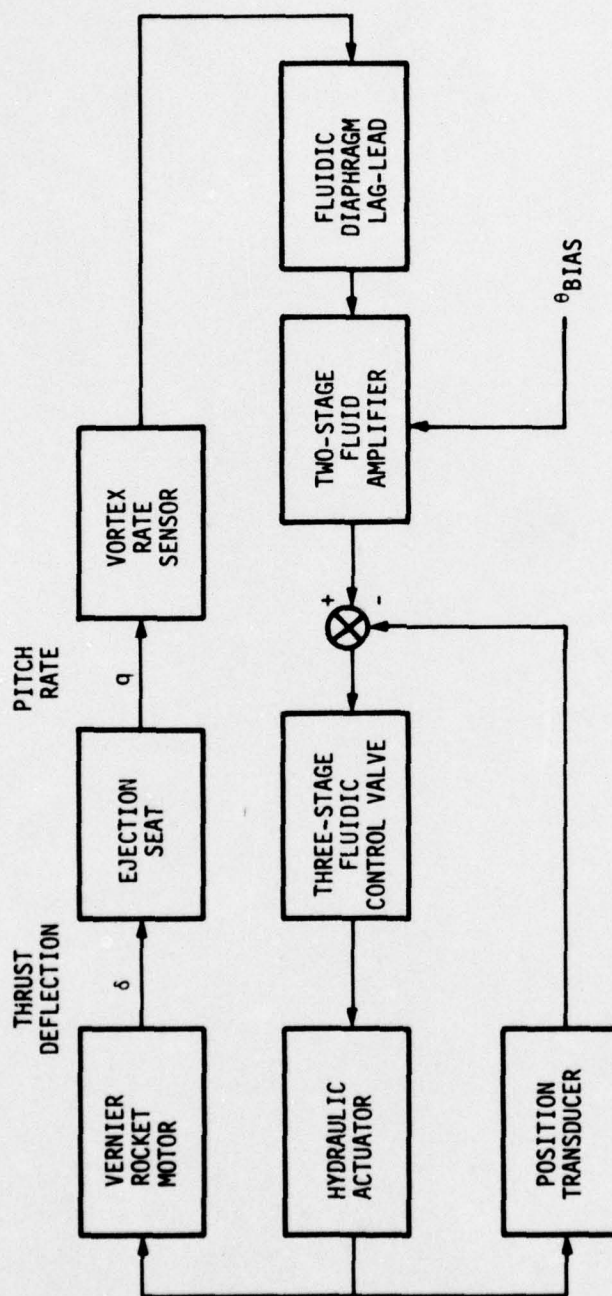


Figure 2. Component Block Diagram

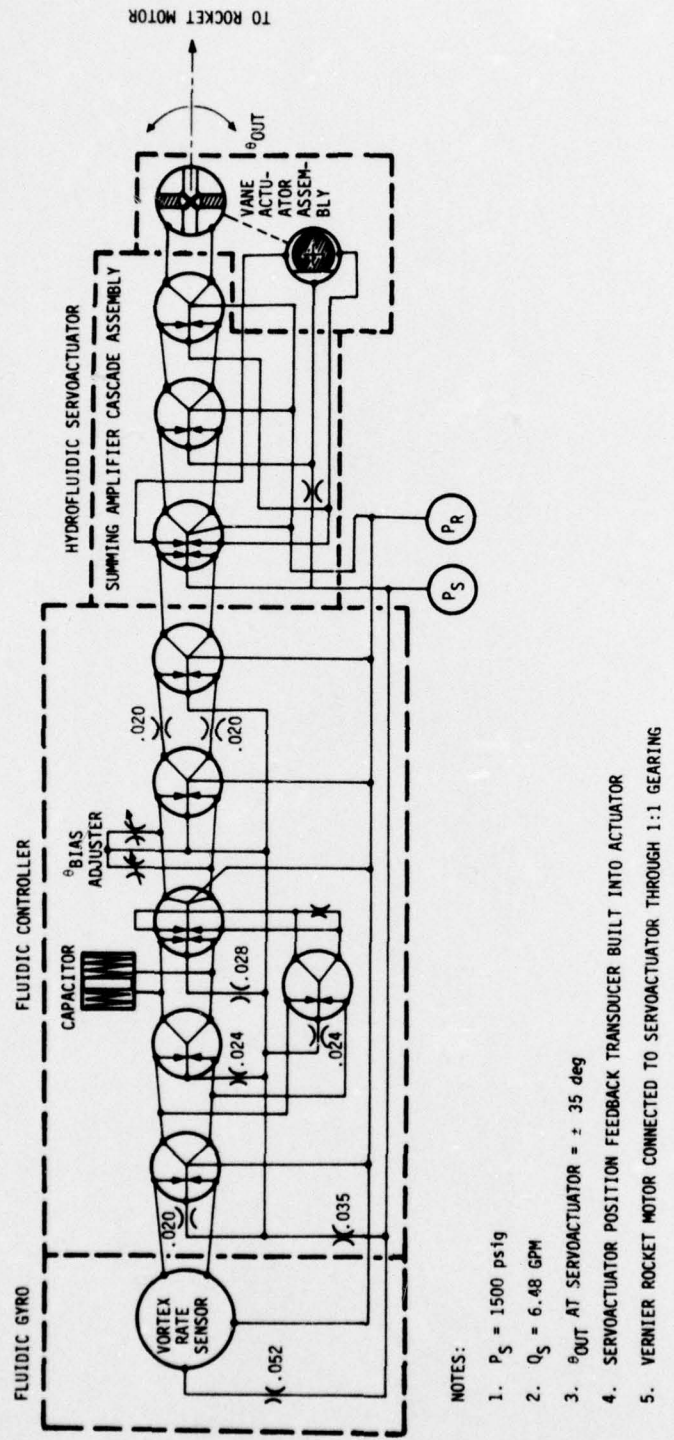


Figure 3a. Detailed Schematic of NAVAIR Breadboard Fluidic Thrust Vector Control

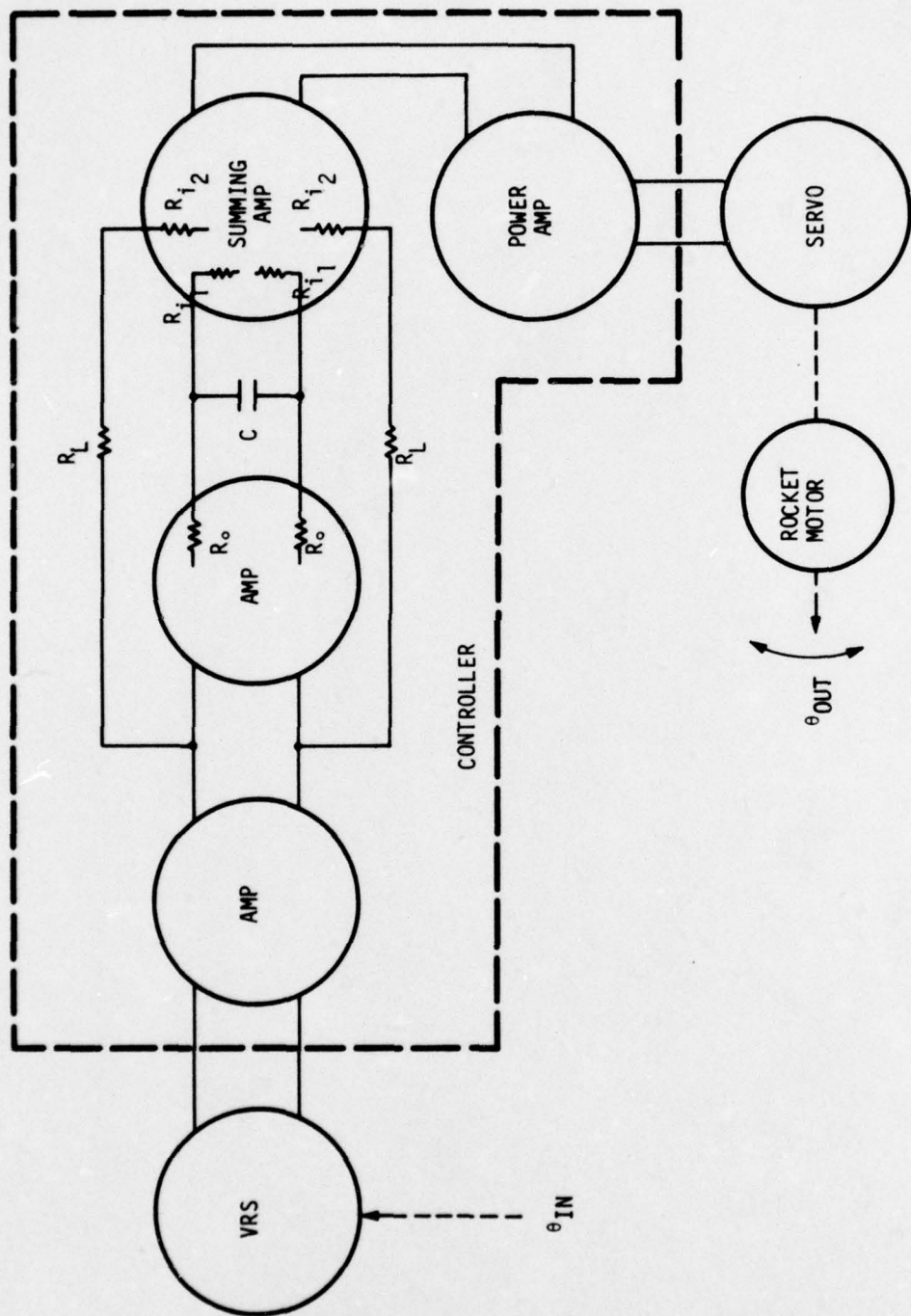


Figure 3b. Controller Schematic Showing Internal Resistance Network

TABLE 1. CONTROL SYSTEM PERFORMANCE

Parameter	Goal	Measured
Deflection Angle (deg)	$\pm 45^\circ$	$\pm 45^\circ$
Slew Rate (deg/sec)	700	750
Torque (in-lb)	40	250
System Gain (at 1 rad/sec)	2.75	2.63
Lag Time Constant (sec)	2.5	2.7
Lead Time Constant (sec)	0.1	0.12
Actuator Bandwidth (Hz)	16	12.5
Rate Sensor Time Delay (sec)	0.010	0.012
Outer Loop (Seat) Phase Margin (deg)	60	45

seat phase margin to be lower than the goal. However, the load and linkage hysteresis and backlash are included in the measured values. Therefore, the seat phase margin of 45° is sufficient to maintain seat stability.

In order to get a better feeling for the comparison of the dynamic design goals and the measured values, consider the system transfer functions. The ideal control system transfer function for stable control is:

$$\frac{q}{\delta_I} (S) = 2.5 \frac{(0.1S + 1)}{S}$$

where

q = Seat pitch rate (deg/sec)

δ = Thrust deflection angle (deg)

I Indicates ideal

S = Laplace transform of frequency (rad/sec)

2.5 = Gain at 1 rad/sec

The S in the denominator indicates the integrator that is necessary to obtain attitude control from the rate sensor. The numerator term cancels out the integrator at 10 rad/sec to allow rate damping to occur at high frequency for stability (Reference 2).

The practical control system has sensor and actuator dynamics which must be designed for ideal performance. The measured transfer function of the breadboard system is

$$\frac{q}{\delta_m} (S) = 2.13e^{-0.012S} \frac{0.12S + 1}{2.7S + 1} \frac{1}{S/78 + 1}$$

2.13 = Gain at 1 rad/sec

where the time delay is caused by the rate sensor, the 2.7 sec lag approximates an integrator, and the 1/78 second lag is caused by the actuator.

Frequency response plots were measured with the complete control system. They are compared with the ideal control law in Figure 4. The responses are closely matched within the required specifications in the frequency range of interest. If these dynamics are added to the seat dynamics, the closed loop system will be stable (Reference 2). The negative slope in the gain

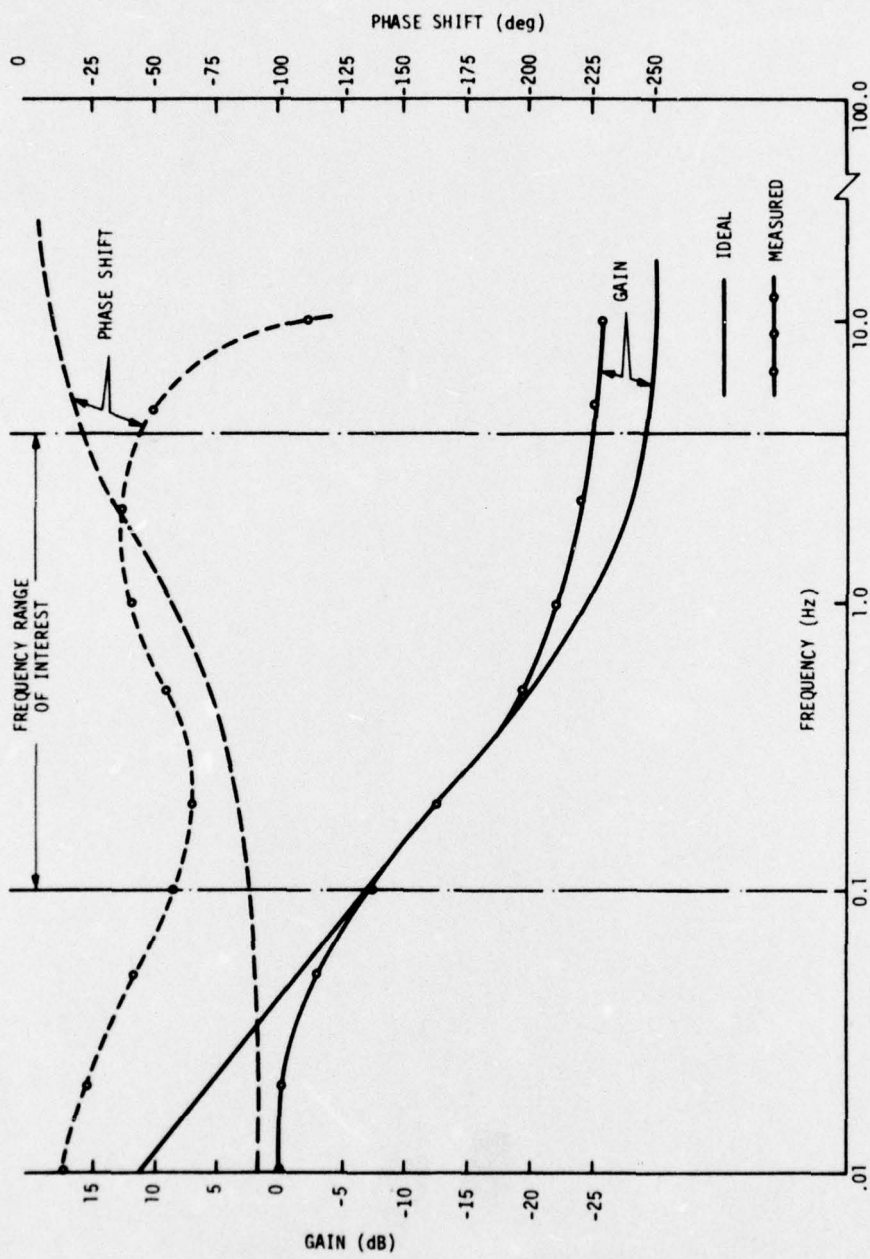


Figure 4. Comparison of Measured and Ideal Controllers

curve provides attitude control during the short flight time of the seat. At frequencies below 0.1 Hz, the real control system memory will leak off, but the seat flight will have been long finished. The high end of the frequency range is the frequency at which the seat cannot respond fast enough to control forces. Therefore, beyond that frequency it does not matter that the control system is not ideal. The 25 deg error in phase shift at 5 Hz causes the drop in phase margin in the outer (seat) loop.

SECTION II

CONTROL SYSTEM DEVELOPMENT

CONTROLLER LOGIC CONCEPT

The fluidic controller (Figure 3b) is of a unique signal summing design which produces gain and the lag-lead signal shaping by combining a straight-through signal and a lagged signal in the jet summing amplifier. The lag time constant depends on the resistance R_o (amplifier output port resistance), R_{i_1} (summing amplifier input port resistance), and the size of the spring-piston capacitor (C). The apparent lead time constant depends mostly on the resistances R_L and R_{i_2} (summing amplifier input port resistance).

In essence, the lag-lead characteristics of the controller are obtained by additively summing the straight-through signal and the lagged signal in the jet summing amplifier. The straight-through path provides the high frequency gain with the resistance R_L set to provide the desired gain. The lag path is set (R_o , R_{i_1} and C) to provide the desired lag corner frequency so that at steady state the unattenuated lag path and straight-through path signals combine to vector the jet summing amplifier to provide the desired d. c. gain.

As the input signal frequency increases, the lag path attenuates to produce the desired controller gain and phase lag characteristics. As the frequency increases to higher values, the lag signal is attenuated so that for all practical purposes it disappears, leaving only the straight-through signal. As

this process develops, the phase lag decreases and the gain attenuation stops with the gain holding constant at the preset high frequency gain. The use of this unique circuit allows the lag and lead characteristics to be adjusted without interacting with each other, as is the case with conventional passive circuitry. Also, the lag-lead characteristics can be generated without causing the d.c. gain attenuation common to passive conventional circuits. Although only four fluid amplifiers are shown in the schematic (Figure 1), the controller was built to take six amplifiers to allow for a significant flexibility in controller gain.

FTVC system d.c. gain is a vital factor in fluidic controller design. An FTVC gain at 0.1 rad/sec (considered close to d.c. gain) of 5 deg rocket motor/deg/sec inertial rate is acceptable with the controller compensation at

$$C(S) = \frac{0.10S + 1}{4.0S + 1}$$

This would presumably yield a 1.0 rad/sec gain of 2.5 deg rocket motor/deg/sec inertial rate. Figure 5 shows the projected dynamic responses of the NADC FTVC using the vortex rate sensor with a 1.56 gpm flow (transport time = 0.011 sec), feasibility controller with the referenced compensation, and the predicted modified servoactuator (1500 psig operation) driving the simulated rocket motor load. From Figure 1 it is seen that, to obtain a 1.0 rad/sec gain of 2.5 deg/deg/sec, a d.c. gain of 9.95 deg/deg/sec is needed instead of the presumed 5 deg/deg/sec. Based on the SRC vortex rate sensor (VRS) gain at a 1.56 gpm flow, a controller d.c. gain of about 2,600 is required to meet the theoretical performance requirements. Although this is considered quite difficult, the breadboard feasibility model NADC controller design is targeted at this goal.

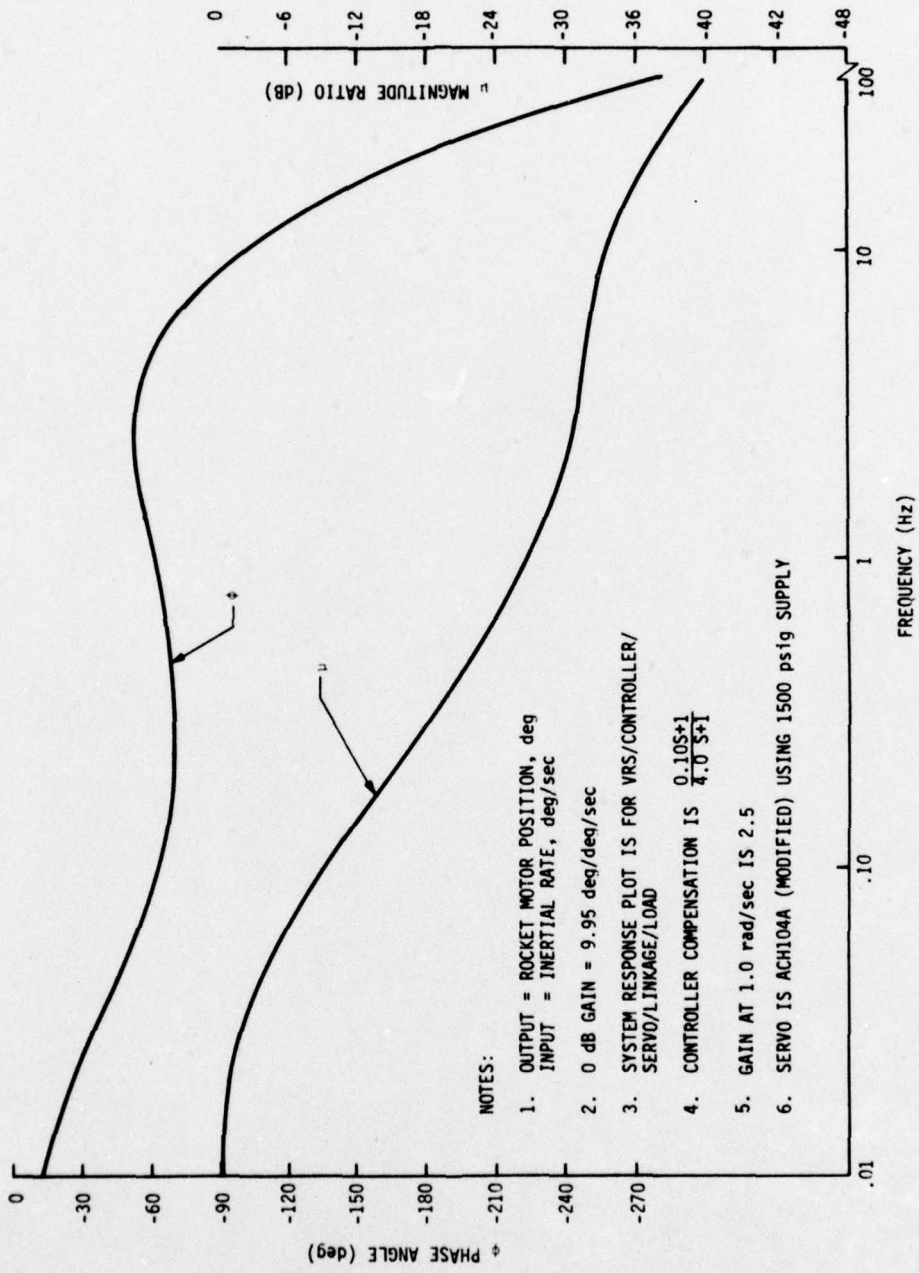


Figure 5. Dynamic Response Design Goal for NAVAIR Fluidic Thrust Vector Control System

BREADBOARD FTVC PRELIMINARY TEST

An initial test was conducted on a breadboard FTVC consisting of the configuration shown in Figure 3. The vortex rate sensor was modified to manifold to the controller. The servoactuator was the production ACH104A1002 (0.81 cu in/rad) vane actuator driving the simulated vernier rocket motor load through a 1:1 gear ratio (not yet changed to the 0.405 cu in/rad actuator).

The breadboard FTVC was mounted on a servoed rate table and powered with hydraulic fluid supplied from a remote test bench. The vortex rate sensor supply was orificed down from the main high pressure supply to provide a 2 gpm VRS power flow. Since the 2 gpm power flow was selected, the SRC rate sensor transport lag was approximately 0.011 sec, and the VRS gain factor driving the controller input fluid amplifier was estimated to be 0.007 to 0.009 psid/deg/sec. The fluidic controller was operated at a supply differential pressure of about 160 psid with supply pressure tuning orifices on all but the power amplifier. The servoactuator was operated at a 1300 psid supply pressure differential. The total supply flow for this breadboard FTVC was estimated at 6 gpm.

The breadboard FTVC was set up to provide a d.c. gain of 9.95 deg (rocket motor)/deg/sec rate. Actually the gain was 6.63 deg/deg/sec since the rocket motor was directly geared to the servo. Since the proper motion ratio was to be added later, all test data at this point were multiplied by 1.5 to permit comparison with design goal performance.

Figure 6 shows the measured dynamic response of the breadboard FTVC compared with the theoretical FTVC. The breadboard controller compensation as measured is approximated by the function

$$C(S) = \frac{0.17 + 1}{3S + 1}$$

so that the resulting 1.0 rad/sec gain is about 1.0 deg/deg/sec instead of the desired 2.5 deg/deg/sec. Since the lag time constant was too large, the value of the capacitance was reduced. Stiffer springs were made for the spring-piston capacitor to reduce the capacitance value. The apparent lead time constant was also too large; therefore, the orifice resistance R_L was increased to move the apparent lead out to a higher frequency. The breadboard FTVC gain in the 5 to 10 Hz region was less than the design goal (see Figure 3b). This is primarily due to the fact that the unmodified servoactuator driven at a 1300 psid supply differential has only a -3 dB bandwidth of about 9 to 10 Hz as compared to the desired 14 to 20 Hz, -3 dB bandwidth. The servo bandwidth was increased when the modified vane actuator was installed.

The zero input signal noise was 0.5 deg/sec peak-to-peak. This was considered quite good since the controller d.c. gain was approximately 1200 psid/psid.

It is concluded that the selected FTVC fluidic mechanization concept is practical. The initial test results were very good; they indicate that the desired dynamic performance can be obtained with appropriate time constant adjustments. Further testing was conducted after the modifications to the servoactuator were accomplished and checked out.

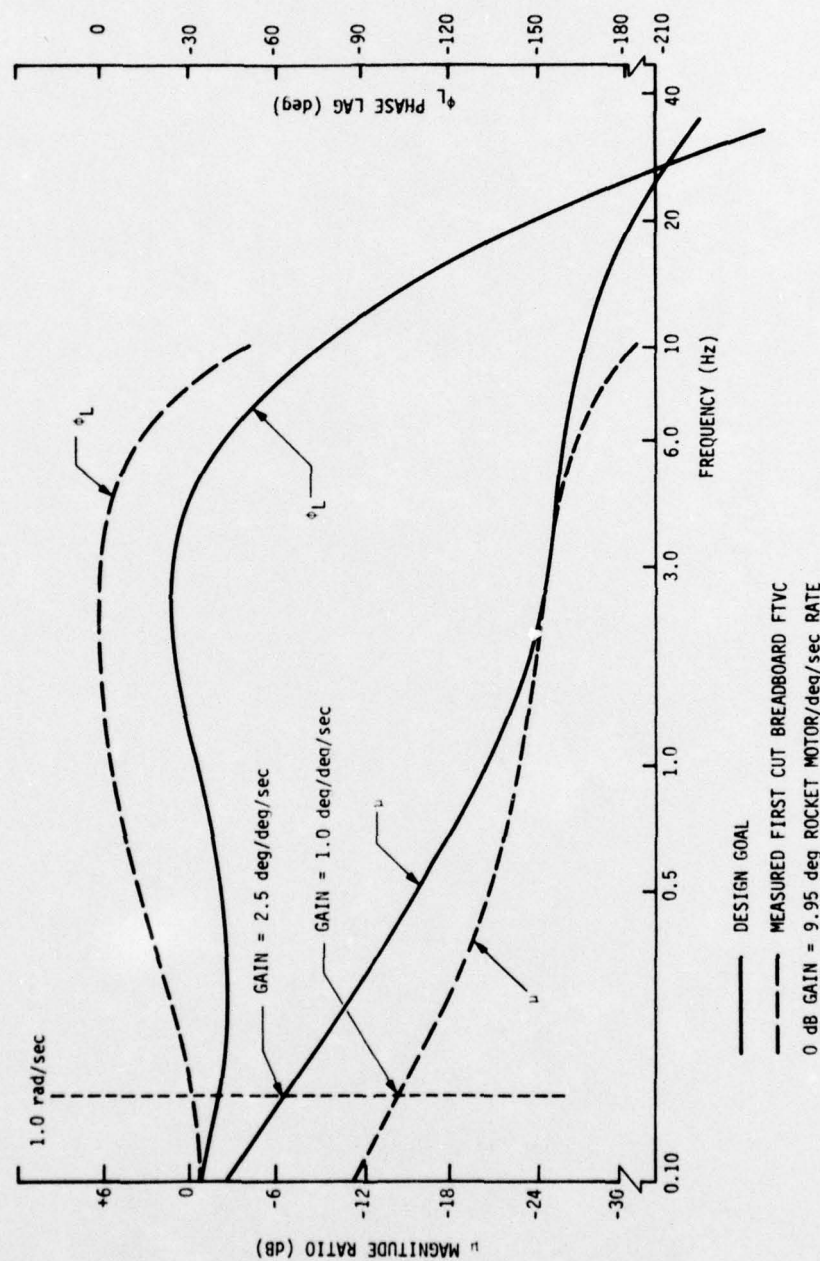


Figure 6. Experimental Dynamic Response for NAVAIR
Fluidic Thrust Vector Control

FTVC FINAL TEST RESULTS

The FTVC operates from a 1500 psig hydraulic supply, using a total supply flow of 6.48 gpm. The servoactuator operates directly from the 1500 psig supply pressure with the vortex rate sensor and fluidic controller using lower level supply pressures. These supply pressures are determined by the orifices in the supply lines which distribute to the VRS and fluidic controller.

The testing was targeted at measurement of FTVC nominal performance characteristics, and little effort was available for off-nominal performance investigation. All tests were conducted with the FTVC supplied with MIL-H-5606 oil from a standard hydraulic test bench. Tests requiring an angular rate input used a servoed rate table. Figure 1 shows a photograph of the FTVC mounted on the test rate table. A special vortex rate sensor manifold was used to orient the vortex rate sensor in the yaw plane (sensor would be in the pitch plane for tactical operation) so that the FTVC mounting to the rate table would provide the minimum load on the table. The FTVC system was tested for basic performance characteristics such as steady state gain, noise, dynamic response, transient response, and null stability. The results of these tests are discussed below.

Steady State Gain

Steady state gain was measured by applying a very low frequency sinusoidal input angular rate and recording rocket motor position versus angular rate on an X-Y plotter. Since the rate table angular deflection was limited by the slack in the hydraulic supply hoses from the test bench, the input rate

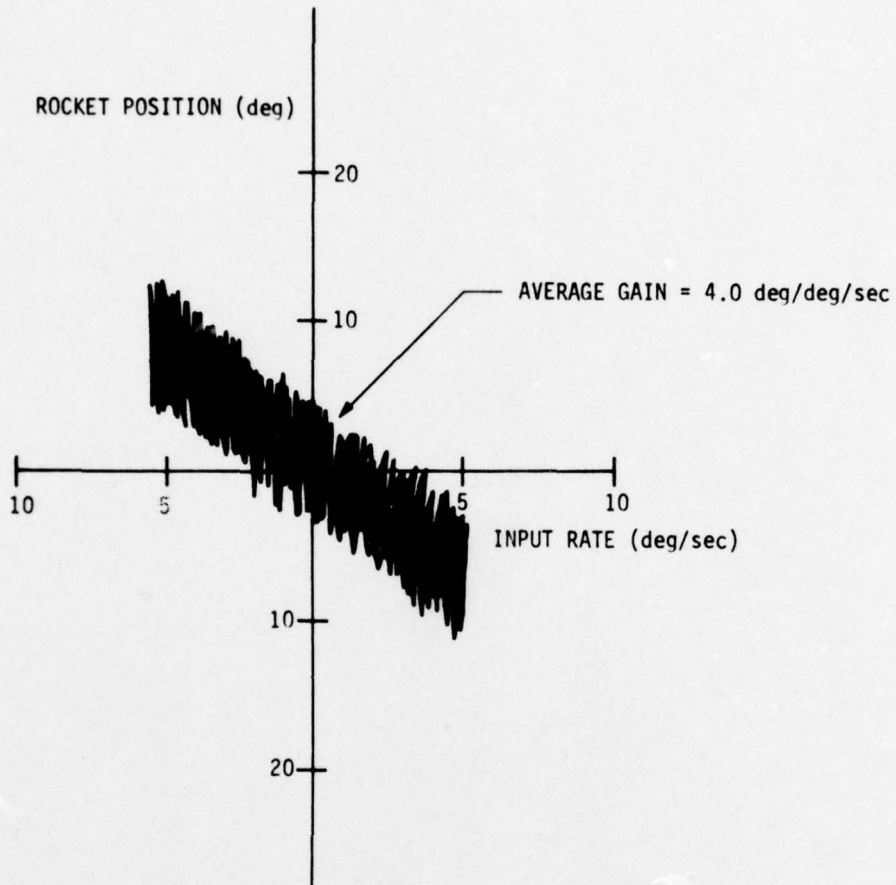
had to be limited to ± 45 deg/sec. Since the lowest programming frequency was 0.010 Hz, the recorded gain factor was about 98.8 percent of the steady state gain factor. Figure 7 shows the measured gain factor at 0.01 Hz as 4.00 deg (rocket motor)/deg/sec (inertial rate). At steady state conditions, the gain factor would be 4.05 deg/deg/sec.

Since the test FTVC used a 1:1 drive between the rocket motor and the servoactuator, the FTVC gain factor for a system using the required 1.5:1 drive between the rocket motor and servoactuator (needed to obtain $\pm 45^\circ$ rocket for $\pm 30^\circ$ servo) would be 6.075 deg/deg/sec. This compares favorably with the design goal steady state gain of 6.57 deg/deg/sec.

Using the measured steady state gain, the gain distribution throughout the FTVC was calculated. Preliminary FTVC testing showed that the vortex rate sensor gain and the hydrofluidic servoactuator gain, as operated in the FTVC system, was 0.0088 psid/deg/sec and 0.72 deg/psid, respectively. The fluidic controller steady state gain was calculated to be 703 psid/psid. The operation of the breadboard fluidic controller was considered good, and the fact that this operation was obtained with a controller gain in excess of 700 was considered a significant accomplishment.

Noise and Null Stability

From the steady state gain testing (Figure 7), the FTVC noise in terms of rocket motor jitter was estimated to be 7.5 deg (peak-to-peak). By monitoring the government furnished equipment (GFE) vortex rate sensor output with the FTVC at null (no input angular rate), it was observed that the rate sensor noise, as displayed in an X-Y plotter, was equivalent to about



NOTES:

1. MIL-H-5606 OIL at 100°F-140°F
2. SUPPLY PRESSURE = 1500 psig
3. SUPPLY FLOW = 6.48 GPM
4. INPUT RATE PROGRAMMING
FREQUENCY = 0.01 Hz

Figure 7. NAVAIR Breadboard FTVC--Steady State Gain

1. 80 deg/sec input rate (peak-to-peak). If the rate sensor noise were amplified by the fluidic controller and if no other noise generators were in the system, the noise as displayed by the servoactuator would be 7.29 deg (peak-to-peak). Since the FTVC noise reflected in terms of input angular rate was equivalent to 1.85 deg/sec, it was concluded that the GFE vortex rate sensor was the primary cause of FTVC system noise. The effect of FTVC system noise on FTVC tactical performance is not known at this time. It is speculated, however, that the noise would have no adverse effects on FTVC control capability. The GFE VRS has a noise level approximately two to three times greater than current Honeywell vortex rate sensors that were fabricated using new techniques which were unavailable to the GFE VRS.

The null stability of the breadboard FTVC was difficult to evaluate due to the short duration (0.50 sec), one-shot mission requirement of the FTVC. Therefore, the only evaluation that could be made was based on null stability during the FTVC bench testing in which the FTVC was operated for long periods of time. In order to set up the breadboard FTVC for testing such factors as steady state gain and dynamic response, it was found that a relatively stable oil temperature condition was necessary to adjust the FTVC to a null condition (rocket motor in mid-position with zero angular rate input). The FTVC null would change if the oil temperature was changing (either increasing or decreasing). The major changes appeared to be when the oil temperature was warming up from room temperature (about 70°F) to the approximate 100°F to 140°F test oil temperature. A brief investigation was conducted and it was observed that the GFE vortex rate sensor output signal changed significantly as the oil temperature changed. Since the vortex rate sensor signal is amplified by a 700 gain controller, it is easy to see that

FTVC null stability is highly dependent upon vortex rate sensor null stability. However, long-term null stability is not too important due to the short mission life (0.50 sec) of the FTVC.

A null offset at time of operation which is different than that at time of calibration would affect the accuracy of the θ_{BIAS} setting. The limited scope of testing did not permit us to test allowable VRS null offset limits which do not adversely affect the θ_{BIAS} signal.

It is believed that the null stability characteristics of the GFE VRS are significantly influenced by the fabrication methods used. For example, the pick-off assembly is a three-piece mechanical assembly. The pick-off is in two pieces with the blade clamped between the two-piece sink by small screws. The current Honeywell fabrication technique is to electroform the pick-off assembly on a sink base plate. This provides a one-piece unit with no possibility of leakage across the pick-off ports. Since this fabrication technique has been in use, VRS null stability has been vastly improved. Also, the new pick-off assembly fabrication technique has allowed the use of four- and eight-port pick-offs. The use of additional ports over the old style two-port pick-off allows variations in signal ports to be averaged which in turn further improves null stability. It is believed that, if the current fabrication techniques had been available at the time the GFE vortex rate sensor was built, the null drifts and offsets due to oil temperature change observed during this test program would not have occurred or would have been minor.

Dynamic Response

Figure 8 compares the breadboard FTVC dynamic response with the design goal response. Driving torque limitations of the available servoed rate table had a considerable influence on the ability to obtain test data at the higher frequencies. This was due to the fact that the hydraulic power hoses from the test bench had to be directly connected to the FTVC because the hydraulic joint in the rate table was of small size and produced an excessively large pressure drop at the 6.48 gpm flow rate used by the FTVC. As a result, these power supply hose connections added a significant loading to the servoed rate table making the desired input rate signal amplitude difficult to maintain over the frequency spectrum of interest.

It is believed that the test servoed rate table torque limitations resulted in considerable distortion of the angular rate wave shape delivered by the rate table. As a result, the BAFCO frequency analyzer used to determine amplitude ratios and phase lags had difficulty in computing the resultant amplitude ratios and phase lags with normal fidelity. This situation is believed to be the cause of scatter in the points of the measured frequency response. Even with the scatter in measured frequency response points, the measured response is considered to be in reasonable compliance with the design goal response.

Transient Response

Figure 9 shows the FTVC system transient response for a simulated outer loop type of test. For this test the θ_{BIAS} adjustment was set so that a 20 deg angular position change of the table (simulates the seat) would cause the

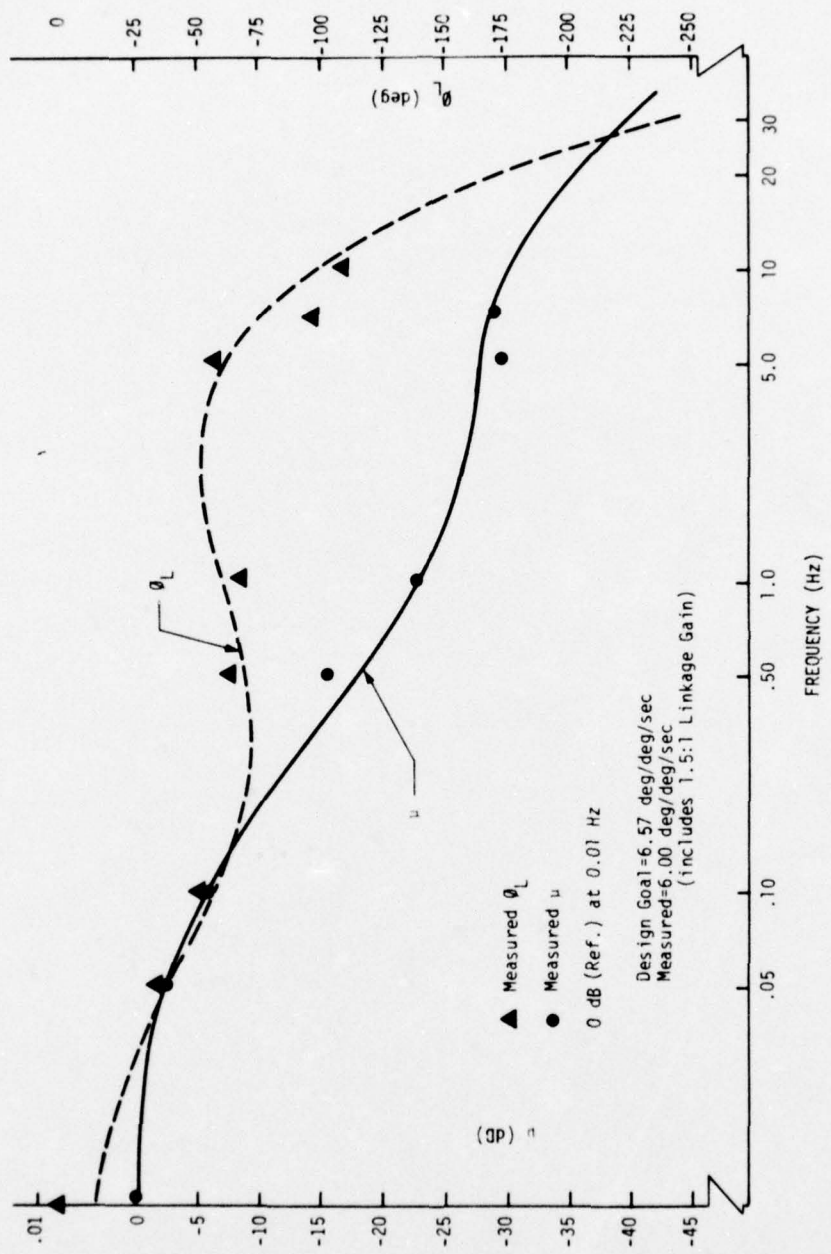


Figure 8. NAVAIR Breadboard FTVC Dynamic Response
 (Design Goal vs. Measured)

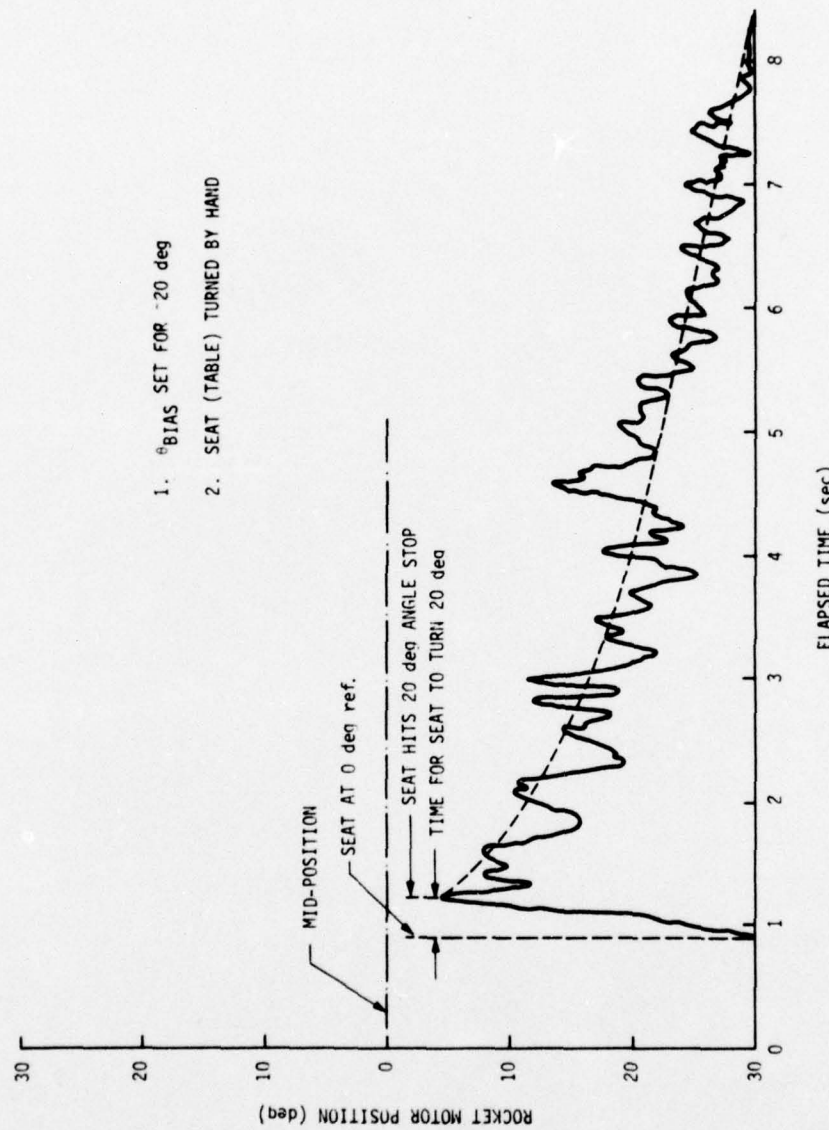


Figure 9. NAVAIR Breadboard FTVC Transient Response for 20 Degree Seat Angle Change

rocket motor to drive to its mid-position. An approximate 20 deg angular travel was marked off and a stop was installed to stop the table. For the purposes of the test, the table was then backed up 20 deg and turned suddenly by hand into the stop. The results of this transient response test are shown in Figure 9. Approximately 0.250 sec was the time to turn the table 20 deg. The rocket motor came off its stop and was within 4 deg of mid-position when the table had turned through 20 deg. If the table travel was exactly 20 deg, it would appear that the 20 deg θ_{BIAS} adjustment was in error by 4 deg (based on the definition of θ_{BIAS}). Since the test had to be conducted in a somewhat cursory manner, the angle measurement was not precise. In any event, this transient motion test demonstrates the principle of the short-term attitude control capability of the breadboard FTVC.

Figure 9 also shows the decay of the fluidic controller signal after the table motion ceased. This decay transient appears to have a time constant of about 2.2 to 2.3 sec which is in reasonable agreement with the controller design goal lag time constant of 2.5 sec. The presence of fluidic noise from the VRS (discussed previously) is also seen on the signal decay transient.

SECTION III

HYDROFLUIDIC SERVOACTUATOR DEVELOPMENT

SERVOACTUATOR CONCEPT

The hydrofluidic servo represents a new concept in hydromechanical servo design. The substitution of hydraulic fluid amplifiers and flowing fluid for the numerous mechanical parts, common to conventional servos, is expected to provide significant advantages in the areas of reliability, environmental hardness, and unit cost.

Figure 10 shows a block diagram of the basic servo concept. The servo consists of a proportional, stream deflected, vented summing fluid amplifier cascade, actuator, and fluidic position feedback transducer. The input signal is provided by any compatible signal interface module. This module can be mechanical to fluidic, electrical to fluidic, pneumatic to fluidic, or a fluidic sensor/controller unit. All fluidic control elements operate with hydraulic fluid obtained from any convenient hydraulic power source. The key component of the servo loop is the summing fluid amplifier cascade. Input signal injection, signal amplification, actuator driving, and position feedback signal summing functions are all performed with this single control element which has no moving parts. The input signal is a differential pressure supplied by the signal interface device.

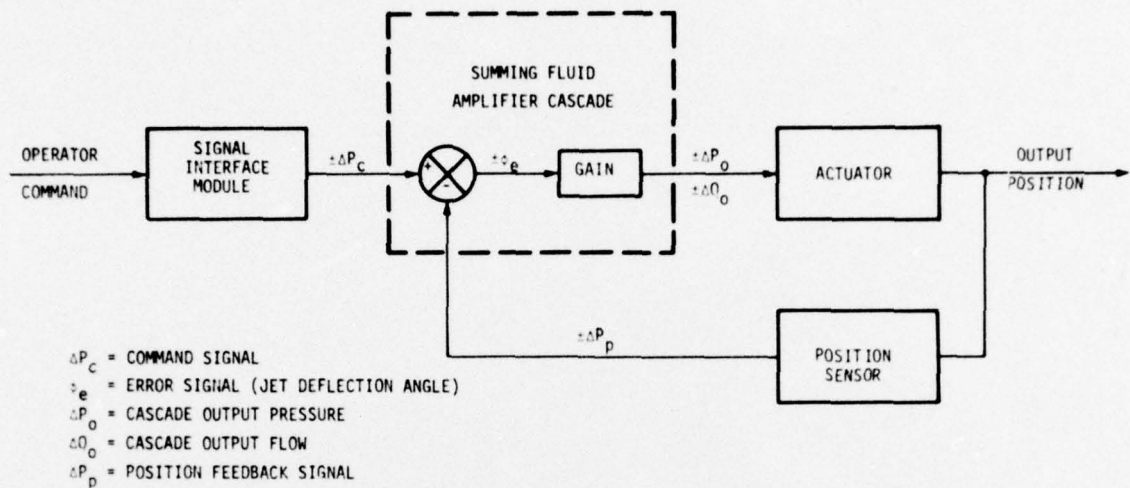


Figure 10. Servoactuator System Diagram

The position feedback signal is a differential pressure supplied by the actuator position feedback transducer. The error signal, which drives the actuator, is the summing fluid amplifier power jet deflection angle. This jet deflection angle is produced by the summation of control stream thrust vectors acting on the summing fluid amplifier power jet.

Figure 10 shows that this concept has eliminated the numerous moving parts common to conventional servo loop mechanizations and has replaced them with dynamic pressure functions. The actuator and position feedback transducer remain as the only moving parts in the servo loop. This simple servo loop mechanization allows a wide variety of performances to be obtained.

from the same servo by varying the servo supply pressure levels. The overall performance capabilities obtained, however, will be determined by the operating supply pressure and the type of hydraulic fluid used.

PRINCIPLES OF OPERATION

The basic operation of the hydrofluidic servoactuator is described from Figure 11. With a supply of pressurized hydraulic fluid applied to the servoactuator and the fluidic controller, power jet and control jet flows are established in the summing fluid amplifier cascade. Power jet flow not used by the fluid amplifier receiver ports is vented to a common return line so that the supply flow remains unchanged whether the servo is re-positioning the actuator or holding a load position. It is important to note that the hydrofluidic servoactuator requires a steady state power flow for operation and is inoperative when the supply flow is cut off.

The input signal to the hydrofluidic servoactuator is supplied by the fluidic controller. This signal, applied to the command ports of the summing fluid amplifier cascade, produces an error signal in the form of power jet deflection angles in the various stages of the cascade. The cascade delivers an output flow rate to the actuator resulting in an actuator angular velocity proportional to the error signal. Actuator rotation causes the fluidic feedback transducers, built into the actuator shaft, to produce a differential

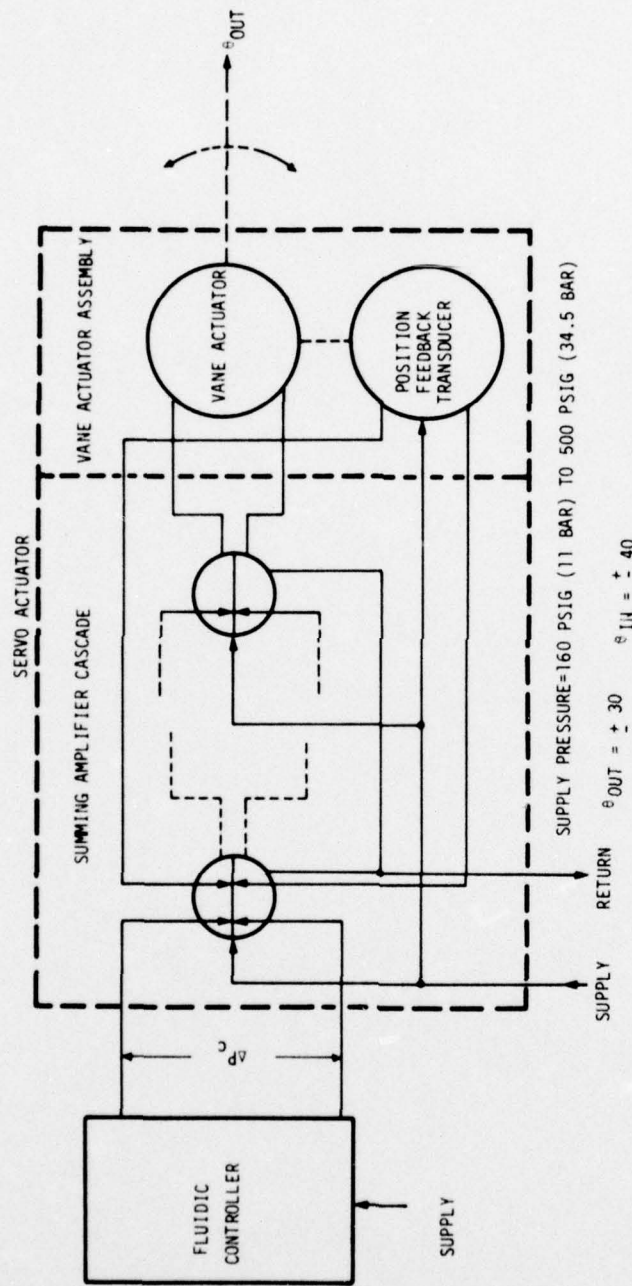


Figure 11. Hydrofluidic Servoactuator Schematic

pressure signal proportional to actuator angular position. This feedback signal, applied to the feedback ports of the summing fluid amplifier cascade, generates a feedback control thrust vector which reduces the cascade power jet deflection angles to zero (null). The cascade output flow rate is reduced to zero and equal static pressures are developed at the actuator ports so that the actuator assumes the angular position commanded by the input signal.

When the actuator is subjected to a change in external load, the accompanying shaft deflection causes the fluidic position feedback transducer to generate an output signal which causes the summing fluid amplifier cascade to produce an output differential pressure to resist the load change. The magnitude of the actuator position change with respect to the magnitude of the load change is determined by the fluidic feedback loop gain. This servo stiffness or torque gradient is a measure of the servo's positional accuracy.

PERFORMANCE REQUIREMENTS

An analysis was conducted to establish a set of performance requirements for the servoactuator. The analysis included computer simulations to investigate the sensitivity of the man/seat trajectory characteristics to actuator slew rates. In addition, a geometric study was conducted to establish the layout and phasing of the control system hardware on the bottom of the ejection seat.

Sensitivity studies were conducted for two "worst case" launch conditions which were established under a previous contract. The launch conditions included the following:

<u>Initial Condition</u>			<u>Low Speed</u>	<u>High Speed</u>
Velocity	V_o	ft/sec	45	1000
Position Angle	θ_o	deg	0	19
Angle-of-Attack	α_o	deg	-90	16.6
Pitch Rate	q_o	deg/sec	-250	213
cg Offset	X_{cg}	in	0	0
	Z_{cg}	in	0	0

Slew Rate

The simulation results indicated that the reduction of the slew rate requirement from 3000 deg/sec to 700 deg/sec did not change the trajectory performance. This reduction to slew rate was possible because of a change in the initial conditions. The 3000 deg/sec requirement was established with a two-inch low cg offset. This was later deemed unrealistic, but the actuator slew rate requirement was not reevaluated.

Torque

Torque requirement was also established for the servoactuator. The computer simulation data for a 700 deg/sec slew rate limit condition indicated that the maximum acceleration torque occurs between 0.250 and 0.260 sec after the seat leaves the rail under the high-speed launch. During this time, the motor acceleration peaks at $138,900 \text{ deg/sec}^2$ and the motor inertia decreases to 0.000573 slug ft². The torque required to cause this condition is 16.7 in-lb.

Efforts to obtain torque information from McDonnel-Douglas (Long Beach) for the friction and thrust misalignment components of recent STAPAC hardware were unsuccessful. References 2 and 3 therefore were used to establish a friction torque of 5.9 in-lb and a thrust misalignment torque of 14.8 in-lb. The latter results from a peak thrust of 742 lb at a nozzle offset of 0.020 in.

The total minimum torque required at the vernier motor is the sum of these components, or 37.4 in-lb. Good servoactuator design practice should include a significant safety factor to eliminate marginal torque performance.

Rotation Angle

The total motor rotation angle of 90 deg is the system requirement. Increased forward rotation of the nozzle ($\psi_{ROCKET} > +45^\circ$) could cause interference between the motor exhaust and the legs of the occupant. Increased aft rotation increases the slew rate requirements while not significantly improving the trajectory performance during ejection.

As indicated below, the neutral position ($\psi_{ROCKET} = 0$) of the current STAPAC motor is perpendicular to the recessed bottom seat surface.

PRELIMINARY TEST RESULTS

Inspection of the servoactuator performance indicated that a modified ACH104A Hydrofluidic Servoactuator could be used. To provide information for potential modifications, a production model ACH104A Hydrofluidic Servoactuator was obtained. This servoactuator was directly coupled to the

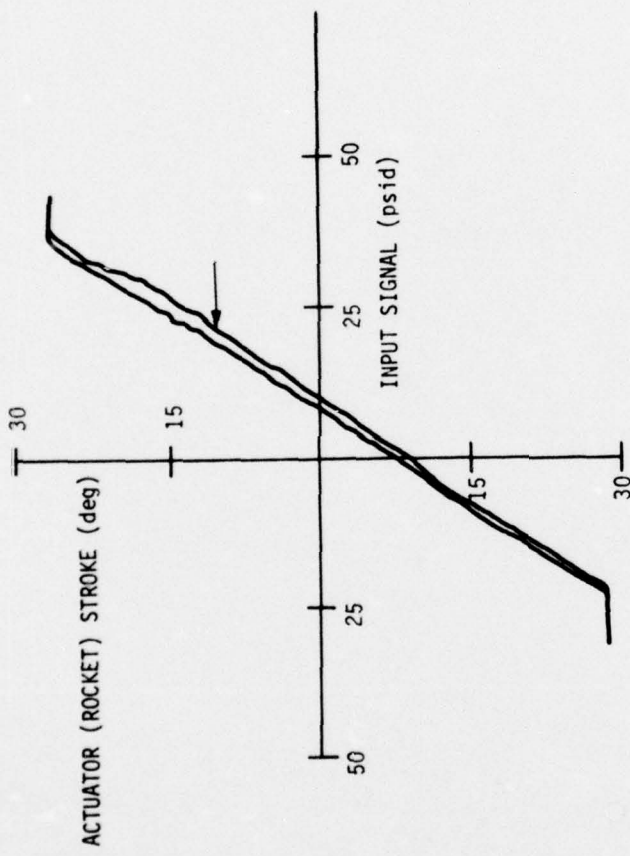
simulated vernier rocket motor by 1:1 gearing. Dynamic response and scale factor tests were made at supply differential pressures up to 2500 psi. Fluid amplifier assembly flow gain data and feedback transducer gain data were extracted to permit a more accurate prediction of potential modified servoactuator performance at high operating pressure. Gear train backlash and motor bearing play of the assembly were also included.

Figures 12 through 15 show the servoactuator scale factors, slew rates, and estimated stall torques for the various supply pressures tested. Figure 16 shows the dynamic responses obtained at the various supply pressures. The stall torque was estimated on the basis of the nominal maximum pressure generated at the actuator and the actuator nominal displacement.

The results of these experiments show that a wide variety of performance capability can be obtained with the servoactuator, depending upon the supply pressure used. During the testing there was no external leakage from the actuator; thus, the sealing process for the fluid amplifier assembly is satisfactory for operation at supply pressures up to 2000 psig. The tests also indicated that jitter (noise) was only about 1.2 percent of the actuator stroke at any pressure tested. This is considered good since the rocket motor jitter includes the servoactuator jitter, gearing backlash, and rocket motor bearing play.

SERVOACTUATOR DESIGN

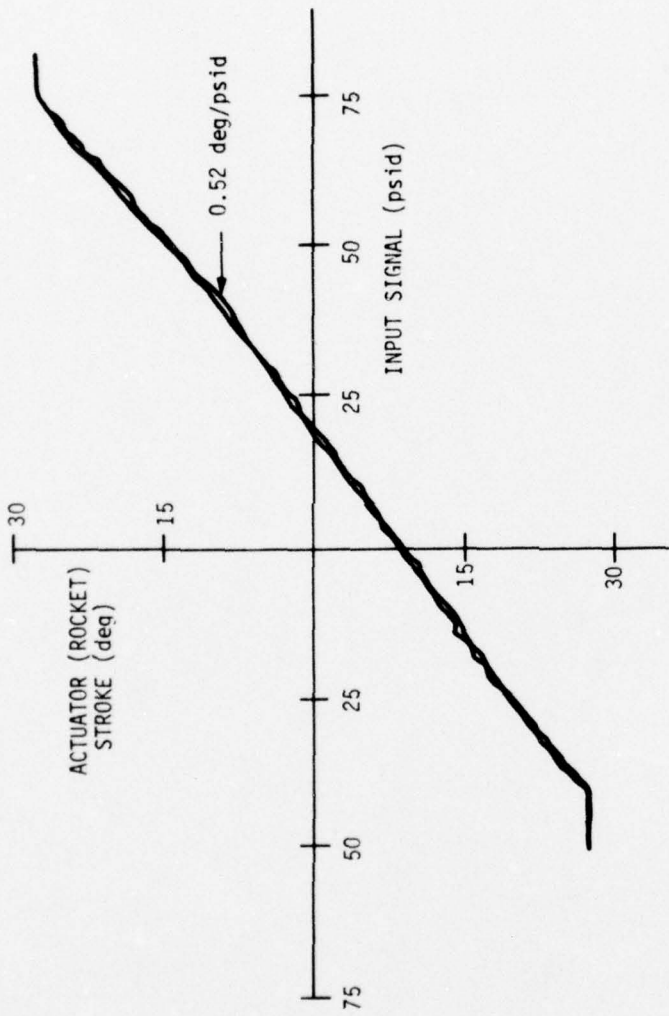
The preliminary test results indicated that it should be feasible to modify an existing production actuator design for compatibility with the vernier rocket motor positioning application.



NOTES:

1. MIL-H-5606 FLUID
AT 100°F - 140°F
2. SIMULATED ROCKET MOTOR DRIVEN
THROUGH 1:1 GEAR TRAIN
3. SUPPLY FLOW = 1.9 GPM
4. SLEW RATE = 132 deg/sec
5. STALL TORQUE = 162 in-lb (MINIMUM ESTIMATION)

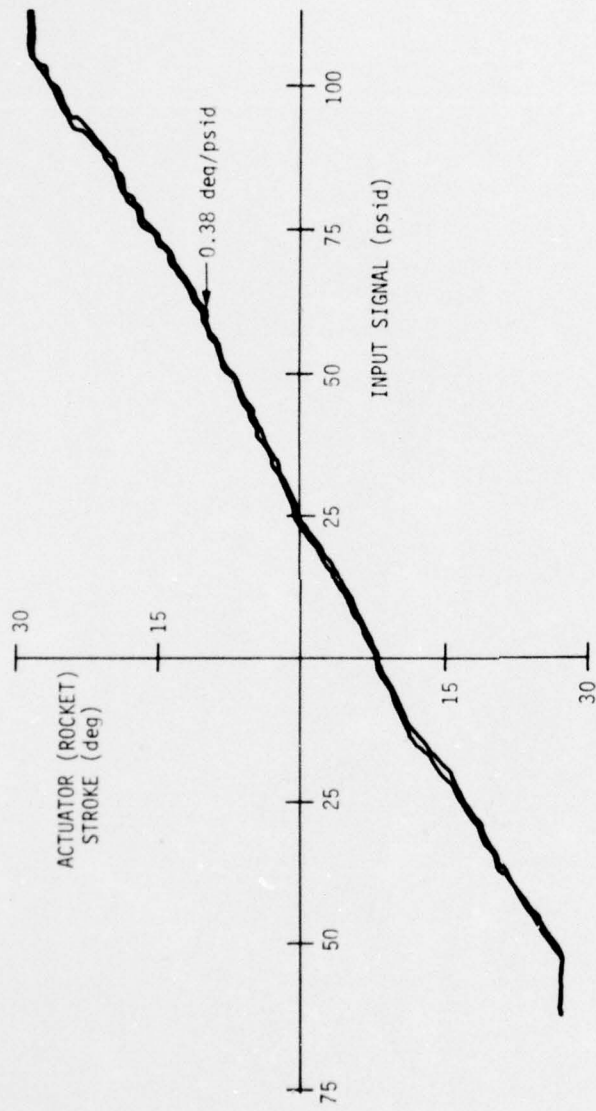
Figure 12. Scale Factor--ACH104A1002 Hydrofluidic Servoactuator,
500 psig Supply Pressure



NOTES:

1. MIL-H-5606 FLUID at 100°F-140°F
 2. SIMULATED ROCKET MOTOR DRIVEN
THROUGH 1:1 GEAR TRAIN
 3. SUPPLY FLOW = 2.79 GPM
 4. SLEW RATE = 188 deg/sec
 5. STALL TORQUE = 324 in-lb (MINIMUM ESTIMATION)
- 1000 psig Supply Pressure

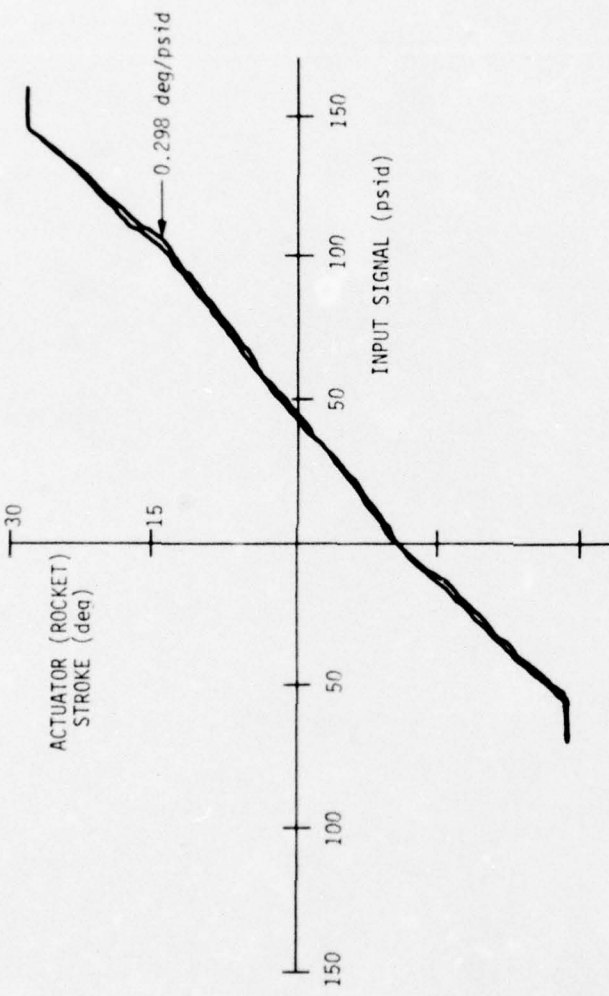
Figure 13. Scale Factor--ACH104A1002 Hydrofluidic Servoactuator,
1000 psig Supply Pressure



NOTES:

1. MIL-H-5606 FLUID at 100°F - 140°F
2. SIMULATED ROCKET MOTOR DRIVEN THROUGH 1:1 GEAR TRAIN
3. SUPPLY FLOW = 3.44 GPM
4. SLEW RATE = 234 deg/sec
5. STALL TORQUE = 486 in-lb (MINIMUM ESTIMATION)

Figure 14. Scale Factor--ACH104A1002 Hydrofluidic Servoactuator,
1500 psig Supply Pressure



NOTES:

1. MIL-H-5606 FLUID at 100°F - 140°F
2. SIMULATED ROCKET MOTOR DRIVEN THROUGH 1:1 GEAR TRAIN
3. SUPPLY FLOW RATE = 3.96 GPM
4. SLEW RATE = 268 deg/sec
5. STALL TORQUE = 648 in-lb (MINIMUM ESTIMATION)

Figure 15. Scale Factor--ACH104A1002 Hydrofluidic Servoactuator,
2000 psig Supply Pressure

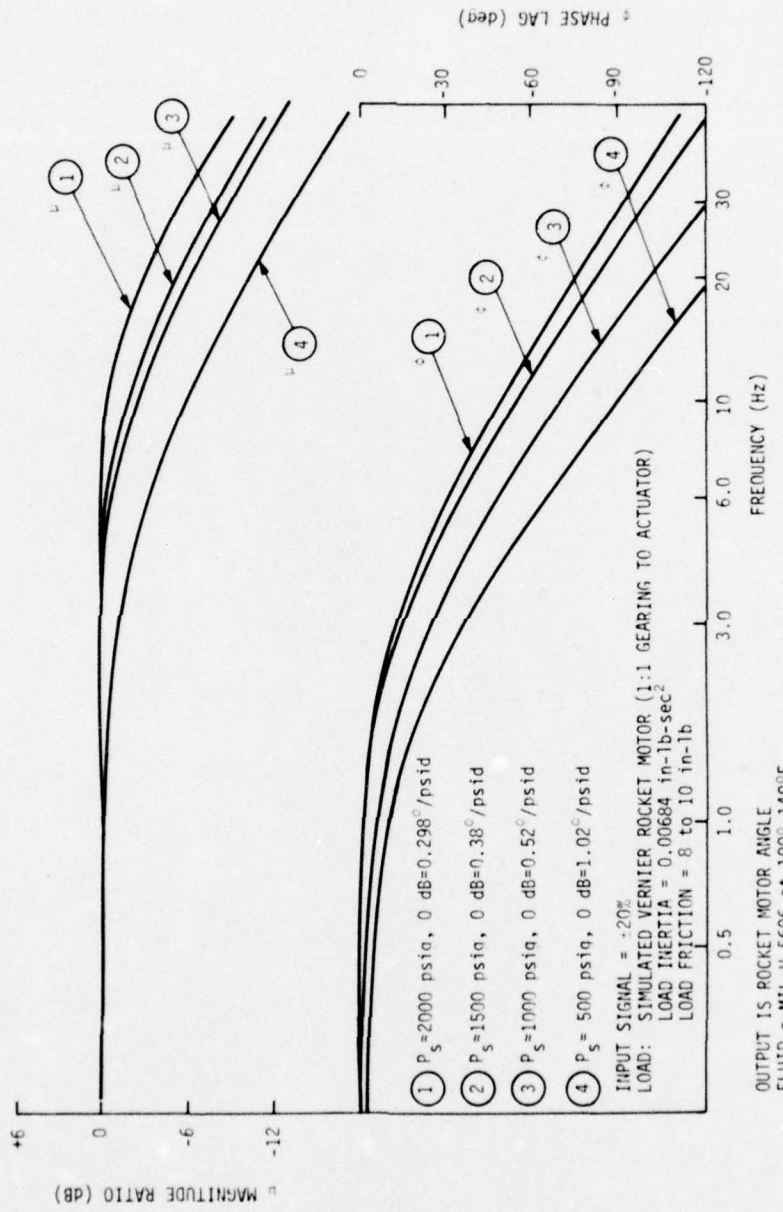


Figure 16. Dynamic Response--Pilot Production
ACH104A1002 Hydrofluidic Servoactuator

An examination of the servoactuator test data indicated that 1500 psig supply pressure was a good operating condition to use as a basis for the modification analysis. Primary reasons were that the supply flow was only about 3.44 gpm as compared with approximately 6 gpm as indicated in Reference 1 and that the servoactuator response bandwidth (based on -3 dB amplitude criteria) was about 14 Hz. This is about equal to that required for the escape system. A review of the vane actuator assembly design indicated that the integral fluidic position feedback transducer feature could not be retained if the vane actuator stroke was increased from the current ± 30 deg stroke to the ± 45 deg required at the rocket motor. However, the ± 45 deg stroke at the rocket motor could be obtained by using a 1.5:1 gear ratio (or linkage) between the actuator and the rocket motor. Therefore, it was decided to retain the integral fluidic position feedback feature in the vane actuator assembly and plan on using a 1.5:1 gear up ratio between the actuator and the rocket motor.

The test data (Figure 14) indicated that for a supply pressure of 1500 psig the resulting servoactuator slew rate was 234 deg/sec. The 1.5:1 gear up could increase this to 351 deg/sec. If the vane actuator displacement was reduced from the current $0.81 \text{ in}^3/\text{rad}$ to $0.0405 \text{ in}^3/\text{rad}$, the slew rate at the rocket motor would be increased to 702 deg/sec. This would be in compliance with the design goal. This approach would provide an estimated stall torque of about 162 in-lb which is well above the 37.4 in-lb requirement. In addition, the reduction in vane actuator displacement would increase the servoactuator open loop gain by 6 dB so that the bandwidth of the modified servoactuator would be in the neighborhood of 20 Hz. It was therefore concluded that the production design ACH104A Hydrofluidic Servoactuator could be modified by reducing the vane actuator volumetric

displacement. This could be done by building a modified actuator body and vane-shaft assembly and substituting these parts for the equivalent parts on the on-hand ACH104A1002 Hydrofluidic Servoactuator. This approach would essentially result in a production proven servoactuator and would reduce design and fabrication costs over those required for a completely new vane actuator assembly.

Design Details

The vane diameter and the actuator body chamber diameter necessary to reduce the actuator displacement from a theoretical $0.81 \text{ in}^3/\text{rad}$ to $0.405 \text{ in}^3/\text{rad}$ were determined. The results indicated that a new actuator body is required. This body would have the same dimensions except that the chamber diameter would be reduced from

$$2.000^{+0.002}_{-0.001} \text{ to } 1.620^{+0.002}_{-0.001}$$

The vane diameter would be reduced from

$$1.988^{+0.003}_{-0.001} \text{ to } 1.608^{+0.003}_{-0.001}$$

The modified vane-shaft assembly can be modified by using on-hand parts and assembling a new vane-shaft assembly.

Minor changes were made to the vane contour to provide the surfaces for the vane to stop on the actuator body abutments at the ± 30 deg travel limits. Because the vane diameter is reduced from that of the production actuator, a slightly different vane contour is necessary. These contour changes could

be machined at the same time that the vane diameter is machined to the reduced dimension. For future production, the modifications would be included in the die casting mold to eliminate machining and to reduce cost. Actuator body, vane, and vane-shaft assembly design sketches were revised according to the desired modifications.

Operating at a 1500 psig supply pressure with reduced vane actuator displacement, the operational characteristics of the modified hydrofluidic servoactuator driving the vernier rocket motor through a 1.5:1 linkage (1.5 deg rocket motor/deg actuator shaft) are predicted to be as follows:

- Supply Flow - 3.44 gpm
- Command Port Pressure Level - 300 psig
- Scale Factor - 0.825 deg rocket motor per psid
- Slew Rate - 702 deg/sec at rocket motor
- Stall Torque - 160 in-lb at rocket motor
- Dynamic Response - -3 dB at approximately 14 Hz

FINAL TEST RESULTS

A surplus ACH104A1002 Hydrofluidic Servoactuator was obtained and supplied to the program for modification purposes. The modification consisted of reducing the vane actuator assembly volumetric displacement from 0.80 cu in/rad to 0.40 cu in/rad. This was accomplished by fabricating a new vane actuator body, reducing the vane diameter of the vane-shaft assembly, and

reducing the height of the rubber insert portion of the vane sealing means. These modified parts were exchanged for the production parts in the surplus servoactuator.

The basic description and operating principles of the servoactuator are given in Reference 6. Design goal performance characteristics for scale factor, stall torque, slew rate, and dynamic response were measured for the 1500 psig operating conditions. The modified actuator was bench tested to evaluate performance under nominal conditions. These results, compared with the design goal characteristics, are shown in Table 2. Usually servoactuator characteristics are specified for a no-load condition. In this case, all tests were performed with the servoactuator driving the simulated vernier rocket motor through a 1:1 gear train.

The test data for several parameters need further discussion. The servo scale factor is influenced to some degree by the command port pressure level since the command jet flow in the summing amplifier cascade assembly contributes to the load impedance of the built-in fluidic position feedback transducer. Therefore, increasing or decreasing the command port ambient pressure level from nominal can increase or decrease the apparent position feedback gain of the transducer resulting in a decreased or increased servo scale factor. Also, manufacturing tolerances on the feedback transducer can cause the same situation, even though the command port ambient pressure is at nominal value.

At the high slew rate of the actuator, it is very difficult to obtain an accurate measurement over the limited stroke of the servo. Scope pictures indicated a slew rate of 470-500 deg/sec. Thus the rocket slew rate will meet specifications with the 1.5:1 gear ratio.

TABLE 2. MODIFIED ACH104A (NAVAIR) HYDROFLUIDIC SERVOACTUATOR TEST RESULTS (Servo Driving Simulated Vernier Rocket through 1:1 Gearing)

Test Parameter	Design Goal/Predicted	Measured Result
Supply Pressure	1500 psig	1500 psig
Supply Flow	3.40 gpm	3.25 gpm
Command Port Pressure Level	25% P _S (375 psig)	400 psig
Scale Factor	0.55 deg/psid	0.52 deg/psid
Linearity	7% Stroke	7% Stroke
Hysteresis	4% Stroke	1.53% Stroke
Threshold	Determined by Load Breakout Friction	Less than Output Jitter
Actuator Jitter (at Rocket)	1.5% Stroke	1.6% Stroke
Full Stroke Signal	+55 psid	+62.5 psid
Stroke	+30 deg	+32.5 deg
Stall Torque	240 in-lb	268 in-lb
Torque Gradient	1300 in-lb/rad	1284 in-lb/rad
Slew Rate	468 deg/sec	470-520 deg/sec
-3 dB Bandwidth	14 Hz	12.5 Hz
As Manufacturing Null Offset	Within 10 deg of Mid-position at 0 ΔP _c	10 deg

The torque gradient (output stiffness) measurement requires that there is no mounting flexure of the torque measurement apparatus. The measurement was made with a lever arm attached to the simulated rocket motor and a large spring scale. It cannot be certified that there was no mounting structure flexure. Thus, the torque gradient measurement is probably better than the measured value.

Figures 17 and 18 show the servoactuator scale factor measurement and the servoactuator loaded dynamic response as indicated in Table 1. The dynamic response shown in Figure 18 is compared with the idealized loaded servoactuator response as used in the computer simulation. The computer simulation neglects the real-life factors of load dynamics (inertial, friction, backlash, etc.). The dynamic response plot was made with significant input signal level; usually the input signal level is held to 10 percent. Based on this plot, the loaded servo -3 dB bandwidth was 12.5 Hz.

Figure 19 shows the scale factor of the servoactuator when driven from the breadboard VSR/Controller unit. The servo scale factor is increased over that shown in Figure 19 and the command port ambient pressure level is 250 psig as compared to 400 psig. This is the characteristic discussed earlier.

The increase in scale factor indicates an apparent reduction in servo position feedback gain. This could imply that the servo loop gain is reduced, assuming that forward loop gain (cascade flow gain) remains relatively constant, and that the servo bandwidth would be somewhat reduced. Preliminary dynamic response tests of the FTVC system do not indicate that to be the case. Servoactuator bandwidth in the FTVC configuration appears to be essentially the same as that obtained during bench testing. It is believed that the reduced command port ambient pressure level reduces feedback transducer load impedance with a resulting decrease in feedback gain. At the same time, the reduced feedback jet flow (in the jet summing amplifier stage) improves the jet deflection sensitivity to the extent that there is an increase in forward loop gain (cascade flow gain) which offsets the feedback

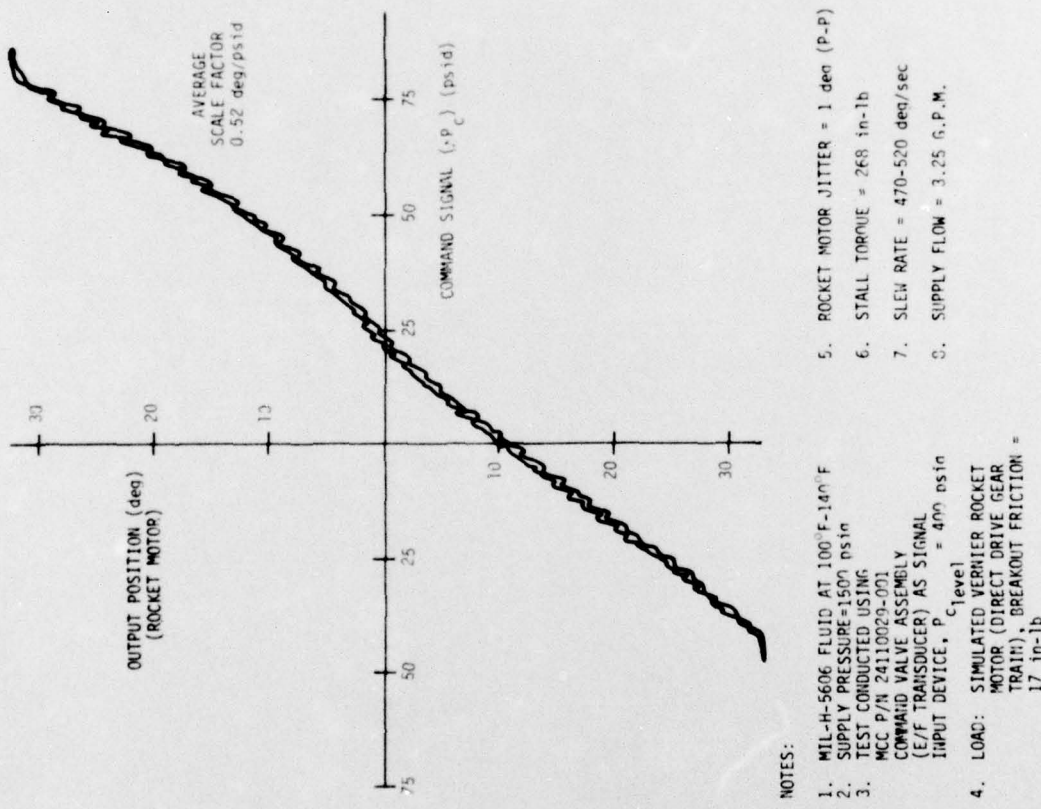


Figure 17. Servo Scale Factor with Hydraulic Bench Input

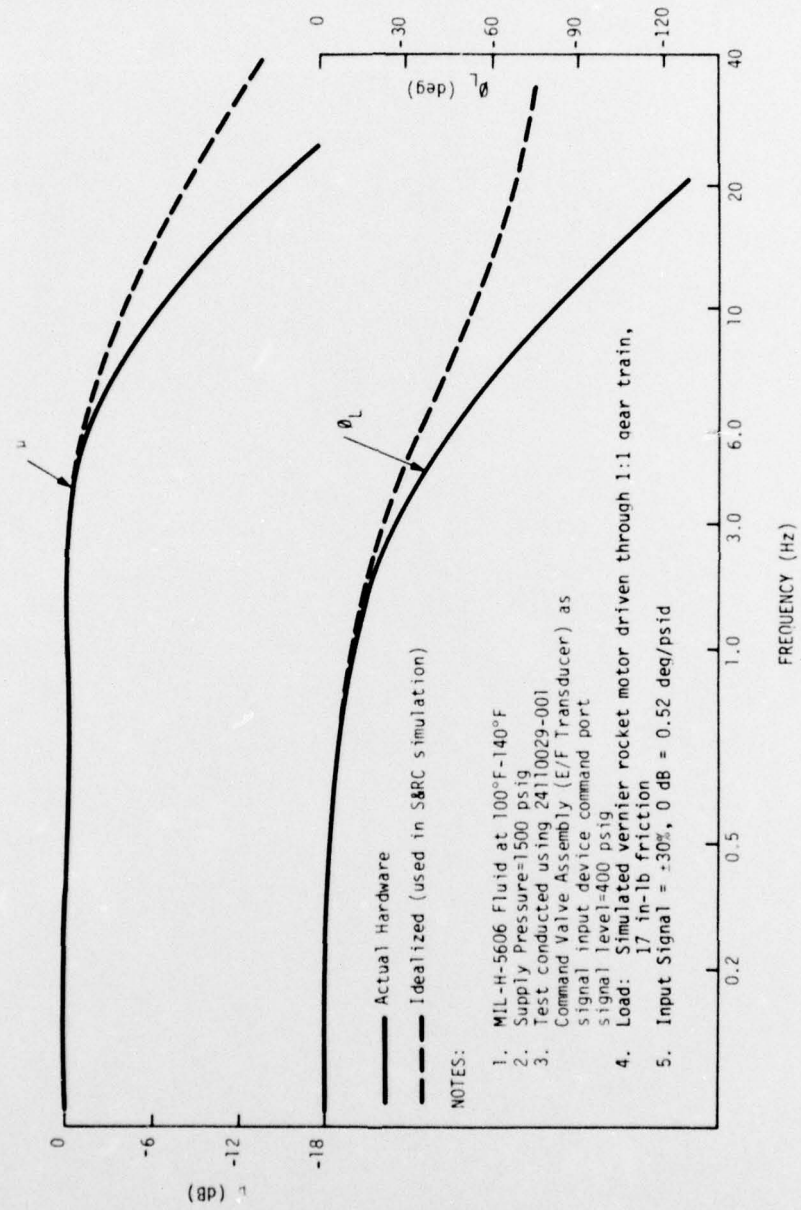


Figure 18. Measured Dynamic Response-- NAVAIR ACH104A
Hydrofluidic Servoactuator

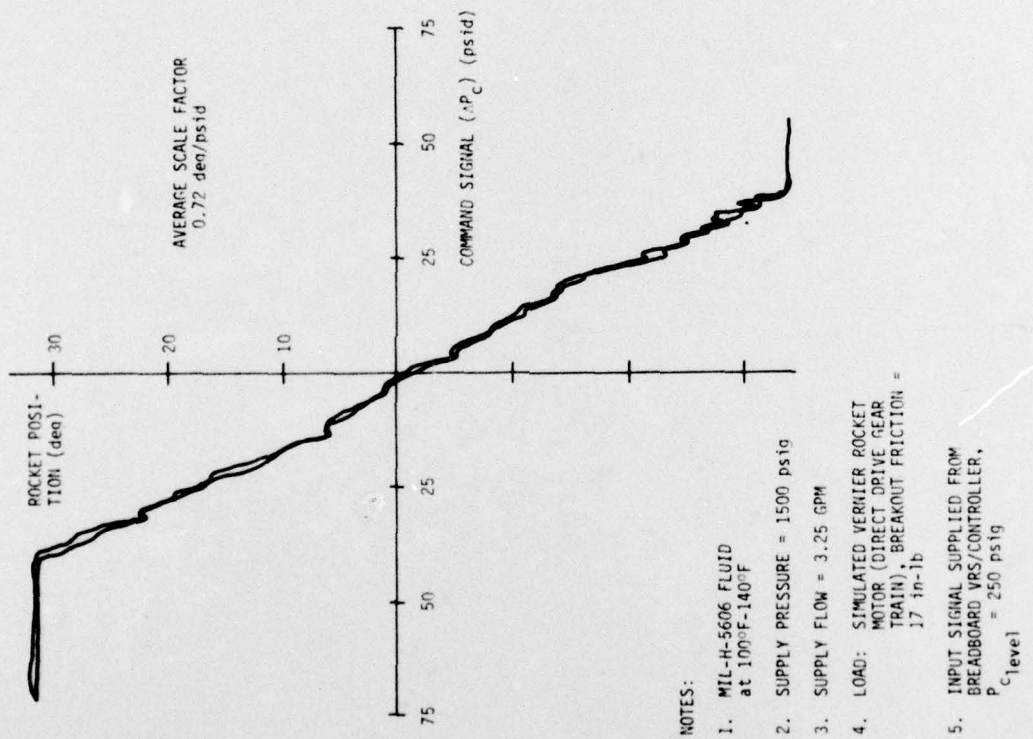


Figure 19. Servo Scale Factor with Controller Input

gain reduction. Servo open loop gain is, therefore, essentially unchanged and the servo closed loop response is essentially unchanged. Since the overall servo performance, other than null offset, apparently is unaffected, the phenomena was not investigated.

In summary, a comparison of the test results and the predicted or design goal characteristics indicates that the modified servoactuator is in general compliance with the design goal performance. The performance parameter test data are considered to be in full compliance with the contract requirements.

SECTION IV

CONCLUSIONS

The following general conclusions are drawn based on the limited scope breadboard FTVC system tests:

1. The breadboard FTVC system demonstrated reasonable compliance with the design goal control law.
2. The feasibility model hydrofluidic servoactuator demonstrated close correlation between design goal/predicted performance and measured performance. At the -3 dB bandwidth, the hydrofluidic servoactuator bandwidth was about 1.5 Hz less than design goal when driving the simulated rocket motor load. It is estimated that an increase in supply pressure from 1500 psig to about 1700 psig would probably increase the bandwidth to design goal requirements.
3. The performance of the breadboard fluidic controller demonstrated that it is practical to build high gain fluidic controllers and that fluidic lag-lead networks can provide the desired degree of short-term memory needed for FTVC application. The test data obtained on the breadboard fluidic controller have provided valuable design information which can be used to improve the controller design and significantly reduce its physical size.

4. The GFE vortex rate sensor demonstrated that fluidic inertial rate sensors have sufficient basic performance capability for the FTVC application. The off-design performance observed at times (null offset and noise) with the GFE vortex rate sensor is considered to be primarily due to the type of fabrication techniques used to construct the rate sensor. New fabrication techniques which have been developed since the GFE vortex rate sensor was built could significantly alleviate the observed null shift and noise characteristics of the vortex rate sensor. It would be highly desirable to replace the GFE vortex rate sensor with a sensor of the same general design performance but built using the new, available fabrication techniques.
5. A follow-on program should be undertaken to conduct more precise laboratory testing before attempting to conduct flight tests under controlled conditions. The program would consist of the following general items:
 - Replace the GFE vortex rate sensor with a similar design being used in Honeywell's UTTAS and HYSAS programs. That VRS uses less flow rate and has better null stability.
 - Adapt the existing STAPAC II rocket motor assembly to the breadboard FTVC and check out FTVC performance with the required rocket motor drive configuration.

- Add a gas generator/accumulator hydraulic power supply to the breadboard FTVC and check out FTVC performance with this type of power unit. Of extremely significant interest would be start-up condition transients. A precise definition of these conditions is needed prior to conducting any controlled flight tests.
- Conduct simulated escape system outer loop tests including a live rocket-firing in the laboratory. These tests are needed to provide performance data which could be vital to insuring a successful flight test demonstration of FTVC feasibility.

REFERENCES

1. Rausch, R. A. and Miller, N. E., "Feasibility Studies of a Hydraulic, Closed Loop, Vernier Rocket Motor Control System for Ejection Seat Stabilization," NADC N00019-75-C-0282, Honeywell, Inc., June 1976.
2. Beale, R. B., "Fluidic Thrust Vector Control for the Stabilization of Man/Ejection Seat Systems," AFFDL-TR-75-105, Honeywell, Inc., September 1975.
3. Moy, H. R. and Nichols, B., "A Rotation and Trajectory Control System for Rocket Catapult Ejection Seats," Douglas Aircraft Paper 3746A presented at 4th National SAFE Symposium, October 1966.
4. Mentzer, J. D., "Dart and Stapac Computer Subroutines," Douglas Aircraft Report DAC33913, August 17, 1967.
5. Burton, R. V., "Fluidic Servoactuator for an Ejection Seat Control System," Unsolicited Proposal letter to Naval Air Systems Command, October 30, 1975.
6. Product Specification, ACH104A-ES01, T&T Sheet 95-8252, Honeywell Mobile Controls Center, 1972.

DISTRIBUTION LIST

	No. of copies
Naval Air Systems Command Washington, D. C. 20361 Attn: Mr. John E. Burns (AIR-52022A)	2
Naval Air Systems Command Washington, D. C. 20361 Attn: Mr. William B. Laughrey (AIR-52022E)	1
Air Force Avionics Laboratory Wright-Patterson AFB, Ohio 45433 Attn: Mr. Richard Jacobs (AFAL/NVN)	1
Naval Air Systems Command Washington, D. C. 20361 Attn: AIR-50174	2
Defense Documentation Center Scientific and Technical Information (DDC) Building No. 5, Cameron Station Alexandria, Virginia 22314 via Naval Air Systems Command Washington, D. C. 20361 Attn: AIR-954	4
Naval Postgraduate School Department of Mechanical Engineering Monterey, California 93940 Attn: Professor T. Sarpkaya	1
Office of Naval Research Arlington, Virginia 22217 Attn: Mr. David S. Siegel (Code 461)	1
Office of Naval Research Arlington, Virginia 22217 Attn: Mr. Stanley W. Doroff (Code 438)	1

	No. of copies
Naval Air Development Center Warminster, Pennsylvania 18974 Attn: Mr. Tor W. Jansen (VTYD)	1
Naval Air Propulsion Test Center Naval Base (Building 600) Philadelphia, Pennsylvania 19112 Attn: Mr. Joseph A. Avbel (Code PE52)	1
Naval Weapons Center China Lake, California 93555 Attn: Mr. Robert E. Fabans (Code 4574)	1
Naval Weapons Center China Lake, California 93555 Attn: Mr. Rolf O. Gilbertson (Code 4044)	1
Naval Weapons Center China Lake, California 93555 Attn: Mr. Nicholas J. Schneider (Code 4040)	1
Naval Ship Research and Development Center Bethesda, Maryland 20034 Attn: Mr. Robert Williams (Code 1605)	1
Naval Weapons Center China Lake, California 93555 Attn: Mr. Robert B. Dillinger (Code 4573)	1
Pacific Missile Range Point Mugu, California 93042 Attn: Mr. Chales Busenkell (Code 3312)	1
Naval Ordnance Laboratory Silver Spring, Maryland 20910 Attn: Mr. C. D. McKindra (Div. 411)	1
Naval Sea Systems Command Washington, D. C. 20360 Attn: Mr. Arthur Chaiken (NSHP-03414)	1

	No. of copies
Naval Ship Research & Development Center Annapolis, Maryland 21402 Attn: Mr. Edwin M. Petrisko (Code 2762)	1
Naval Ship Research & Development Center Annapolis, Maryland 21402 Attn: Mr. John L. Joynes (Code 2781)	1
Naval Ship Research & Development Center Annapolis, Maryland 21402 Attn: Mr. Larry F. Marcus (Code 276)	1
Air Force Office of Scientific Research 1400 Wilson Boulevard Arlington, Virginia 22209 Attn: Mr. Milton Rodgers (AFOSR/NAM)	1
Air University Air Force Institute of Technology Wright-Patterson AFB, Ohio 45433 Attn: Dr. Milton E. Franke (AFIT/ENM)	1
AF Flight Dynamics Labotatory Wright-Patterson AFB, Ohio 45433 Attn: Mr. Harry M. Snowball (AFFDL/FGL)	1
AF Flight Dynamics Laboratory Wright-Patterson AFB, Ohio 45433 Attn: Mr. Max Lipscomb	1
AF Aero Propulsion Laboratory Wright-Patterson AFB, Ohio 45433 Attn: Mr. Charles Bentz (AFAPL/TBC)	1
Air Force Weapons Laboratory Kirtland AFB, New Mexico 87117 Attn: Capt. Ervin P. Jaskolski (AFWL/SRA)	1
Office of Chief of Research & Development Washington, D. C. 20310 Attn: Major Robert A. Burns (DARD-ARP-P)	1

	No. of copies
Harry Diamond Laboratories 2800 Powder Mill Road Adelphi, Maryland 20783 Attn: DRXDO-PP (Mr. L. Cox)	1
Harry Diamond Laboratories 2800 Powder Mill Road Adelphi, Maryland 20783 Attn: DRXDO-RCA (Mr. F. Manion)	1
Harry Diamond Laboratories 2800 Powder Mill Road Adelphi, Maryland 20783 Attn: DRXDO-RCA (Mr. T. Drzewiecki)	1
Harry Diamond Laboratories 2800 Powder Mill Road Adelphi, Maryland 20783 Attn: DRXDO-RCD (Mr. R. Gottron)	1
Harry Diamond Laboratories 2800 Powder Mill Road Adelphi, Maryland 20783 Attn: DRXDO-RCD (Mr. J. Joyce)	1
Army Materiel Command Washington, D. C. 20315 Attn: AMCRD-TP (Mr. J. Hughes)	1
U. S. Army Air Mobility R&D Laboratory Fort Eustis, Virginia 23604 Attn: SAVDL-EU-AM (Mr. G. Fosdick)	1
Army Missile Command Redstone Arsenal, Alabama 35809 Attn: AMSMI-RGC (Mr. W. Griffith)	1
Army Missile Command Redstone Arsenal, Alabama 35809 Attn: AMSMI-RGC (Mr. J. Williams)	1

	No. of copies
Army Missile Command Redstone Arsenal, Alabama 35809 Attn: Mr. Paul Jacobs	1
Army Missile Command Redstone Arsenal, Alabama 35809 Attn: Mr. B. J. Clayton	1
Army Missile Command Redstone Arsenal, Alabama 35809 Attn: Mr. G. F. Hall	1
Army Weapons Command Rock Island, Illinois 61201 Attn: Mr. Verlin Baumgarth (SWERR-W-A)	1
Army Weapons Command Rock Island, Illinois 61201 Attn: Mr. Philip Townsend (SWERR-W-A)	1
Army Weapons Command Rock Island, Illinois 61201 Attn: Mr. Delmar Ackerman (SWERR-T)	1
Army Tank Automotive Command Warren, Michigan 48090 Attn: Mr. Gregory Arbutian (AMSTA-RGD)	1
Army Mobility Equipment R&D Center Fort Belvoir, Virginia 22060 Attn: Mr. Robert N. Ware (DRXFB-EM)	1
Naval Ship Research & Development Center Bethesda, Maryland 20034 Attn: Technical Library (Code 5643)	1
Picatinny Arsenal Dover, New Jersey 07801 Attn: Dr. Albertus E. Schmidlin (SMUPA-ND-C-C)	1

	No. of copies
Watervliet Arsenal Watervliet, New York 12190 Attn: Mr. John A. Barrett	1
Frankford Arsenal Philadelphia, Pennsylvania 19137 Attn: Mr. Robert A. Schaffer (SMUFA-J-6100)	1
NASA/Langley Research Center Hampton, Virginia 23365 Attn: Mr. Richard F. Hellbaum (MS 494)	1
NASA/Langley Research Center Hampton, Virginia 23365 Attn: Mr. H. Douglas Garner (MS 494)	1
NASA/Lewis Research Center 21000 Brook Park Road Cleveland, Ohio 44135 Attn: Mr. Vernon D. Gebben	1
NASA/Ames Research Center Moffett Field, California 94035 Attn: Mr. Dean Chisel (N242-3)	1